Flavin-N5OOH: A powerful nucleophile and base in nature

Qiaoyu Zhang[†], Qianqian Chen, Sason Shaik[§]*, Binju Wang[†*]

[†]State Key Laboratory of Physical Chemistry of Solid Surfaces and Fujian Provincial Key Laboratory of Theoretical and Computational Chemistry, College of Chemistry and Chemical Engineering and Innovation Laboratory for Sciences and Technologies of Energy Materials of Fujian Province (IKKEM), Xiamen University, Xiamen 361005, P. R. China.

[§]Institute of Chemistry, The Hebrew University of Jerusalem, 9190407, Jerusalem, Israel.

Abstract

Flavoenzymes can mediate a large variety of oxidation reactions via the activation of oxygen. As such, the chemistry of flavoenzymes is an important field that has not yet attained its full scope/recognition. Normally, the O_2 activation occurs at the C4a site of the flavin cofactor, yielding the flavin C4a-(hydro)hydroperoxyl species in monooxygenases or oxidases. Using extensive MD simulations, QM/MM calculations and QM calculations, our studies reveal the formation of the common nucleophilic species, flavin-N5OOH, in two distinct flavoenzymes (RutA and EncM). Our studies show that flavin-N5OOH acts as a powerful nucleophile that promotes C–N cleavage of uracil in RutA, and a powerful base in the deprotonation of substrates in EncM. We reason that flavin-N5OOH can be a common reactive species in the superfamily of flavoenzymes, which accomplishes the generally selective general base catalysis, and the C–X (X= N, S, Cl, O) cleavage reactions that are otherwise challenging by solvated hydroxide ion base. These results expand our understanding of the chemistry and catalysis of flavoenzymes.

Keywords: Oxygen activation, Flavoenzymes, QM/MM, Flavin-N5OOH

INTRODUCTION

Flavin-dependent enzymes catalyze a panoply of chemical transformations that are essential for all types of living organisms[1-10]. To date, over 100,000 protein sequences have been classified as flavin-enzymes[1, 2, 7, 11, 12]. The typical reactions catalyzed by flavin-enzymes cover: dehydrogenation[13-15], monooxygenation[3, 11, 16-21], halogenation/dehalogenation reactions[22-26], and photochemical reactions[27-31]. As such, flavoenzymes are vital to metabolic and synthetic processes in biology.

Akin to metalloenzymes[32-34], the flavin-enzyme can perform O_2 activation, which leads to the formation of reactive flavin-oxygen intermediates for various oxygenation reactions[2, 7, 11, 17, 35] .For instance, the O_2 activation at the C4a site of the flavin cofactor affords the flavin C4a-hydroperoxy (Flavin-C4aOOH) species or the flavin C4a-peroxo anion (Flavin-C4aOO$^-$) species (Fig. 1a), which were recognized as the key intermediates of flavin-dependent monooxygenases[7, 12, 21, 36-46].

In addition to Flavin-C4aOO(H), Moore and coworkers characterized the versatile enterocin biosynthetic flavoenzyme, EncM, that activates O_2 and generates the uncommon species of flavin-N5-oxide (labelled as Flavin-N5O)[47-52], as shown in Fig. 1b. It was proposed that the O_2 activation in EncM may first lead to the Flavin-N5OOH species, which is followed by the O–O cleavage to generate the Flavin-N5O species. Subsequently, Flavin-N5O attacks the C4 position of the deprotonated substrate analogue (Fig. 1b)[48]. Using O_2-pressurized X-ray crystallography (Fig. S1), Teufel and coworkers characterized the high-resolution structure of EncM, in which O_2 is in close proximity to N5[48]. In addition, density-functional theoretic (DFT) calculations showed that the generation of Flavin-N5O via the Flavin-N5OOH intermediate is kinetically and thermodynamically feasible[48]. In a recent work, Teufel and coworkers investigated the C–N cleavage of uracil by the flavoenzyme RutA[53, 54]. Unlike the Flavin-N5O species invoked for the oxidative rearrangement in flavin-enzyme EncM, an unusual flavin-N5-peroxide (Flavin-N5OO$^-$) species was proposed to be the nucleophile for catalysis of RutA (Fig. 1c). In fact, the Flavin-N5OO$^-$ species was proposed to be the reactive species for many other non-redox transformations[16, 53, 55-58]. However, as yet no evidence is available to support the formation of Flavin-N5OO$^-$ species, either

experimentally or computationally.

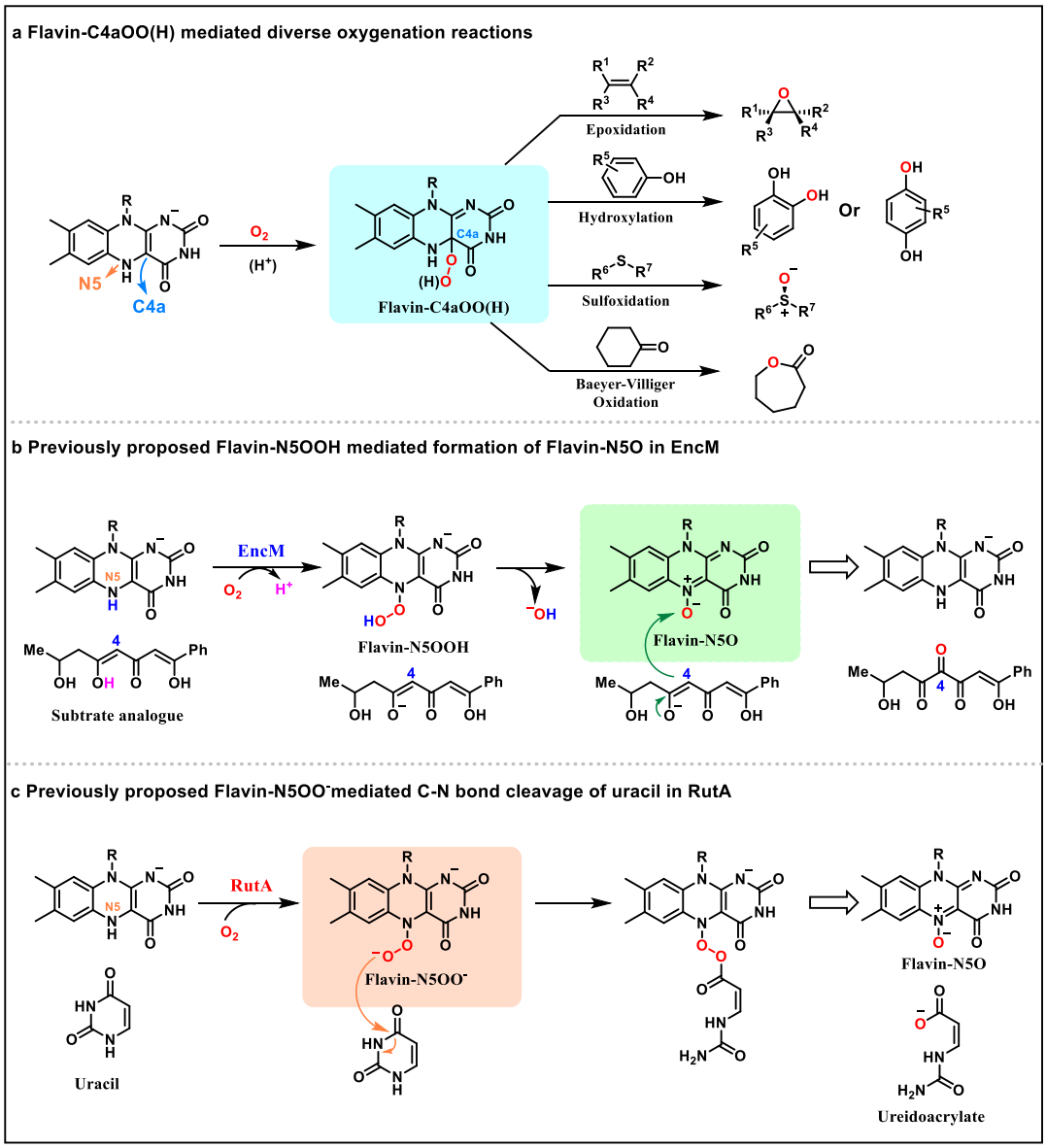

Fig. 1 | Potential active species in flavoenzymes. a Flavin C4a-hydroperoxide (Flavin-C4aOOH) or Flavin C4a-peroxide (Flavin-C4aOO^{-}) as the active species for diverse oxygenation reactions. **b** A proposed mechanism for the formation of the Flavin-N5O species and the substrate oxygenation at the C4 position during the flavoenzyme EncM catalysis. **c** A proposed mechanism for the formation of the Flavin-N5O species and the C–N cleavage of uracil in the flavoenzyme RutA[53].

To explore the active species in EncM and RutA (Fig. 1), we performed molecular dynamics (MD) simulations, quantum mechanical/molecular mechanical (QM/MM) calculations and QM calculations. Our study demonstrates that O_2 activation by

flavoenzymes RutA and EncM take place via the common active species of the Flavin-N5OOH species, which function as the powerful nucleophile in the RutA-catalyzed C–N cleavage of uracil and as a powerful base in EncM-catalyzed C4-ketolation. These reactions suggest that the singlet-state Flavin-N5OOH species may function as a common species in nature (see Fig. S2), and mediate a large variety of the non-redox transformations.

Results

The X-ray crystal structure of RutA (PDB ID: 6TEG) in complex with the flavin mononucleotide (FMN), uracil and O_2 has been successfully crystallized by Teufel et al. in 2020[53]. This structure enables us to probe the molecular mechanism of RutA. As indicated in the crystal structure (Fig. 2a), the C4a of FMN is relatively distant from O_2 (distance: 3.1 Å), while N5 of FMN is significantly closer to O_2 (distance: 2.1 Å). As such, the catalytic reaction may lead to the formation of Flavin-N5OO$^-$ or Flavin-N5OOH, instead of Flavin-C4aOO$^-$ or Flavin-C4aOOH. To ascertain the mechanism, we have used QM model calculations to test the uracil attack by the tentative Flavin-C4aOOH in RutA. We found that the process, including the OH$^-$ moiety transfer from Flavin-C4aOOH to uracil, is highly endothermic ~26.0 kcal/mol (see Fig. 2b), and thus thermodynamically forbidden. In addition, we also investigated the nucleophilic attack of uracil by Flavin-C4aOO$^-$ species, and found that the so-formed Criegee-intermediate is highly unstable, lying 10.3 kcal/mol above the Flavin-C4aOO$^-$ species. Furthermore, this Criegee-intermediate mediated C–N cleavage of uracil is endothermic by 10.0 kcal/mol and requires a barrier of 13.1 kcal/mol, thus indicating that the intermediate is a dead-end (see Fig. 2c).

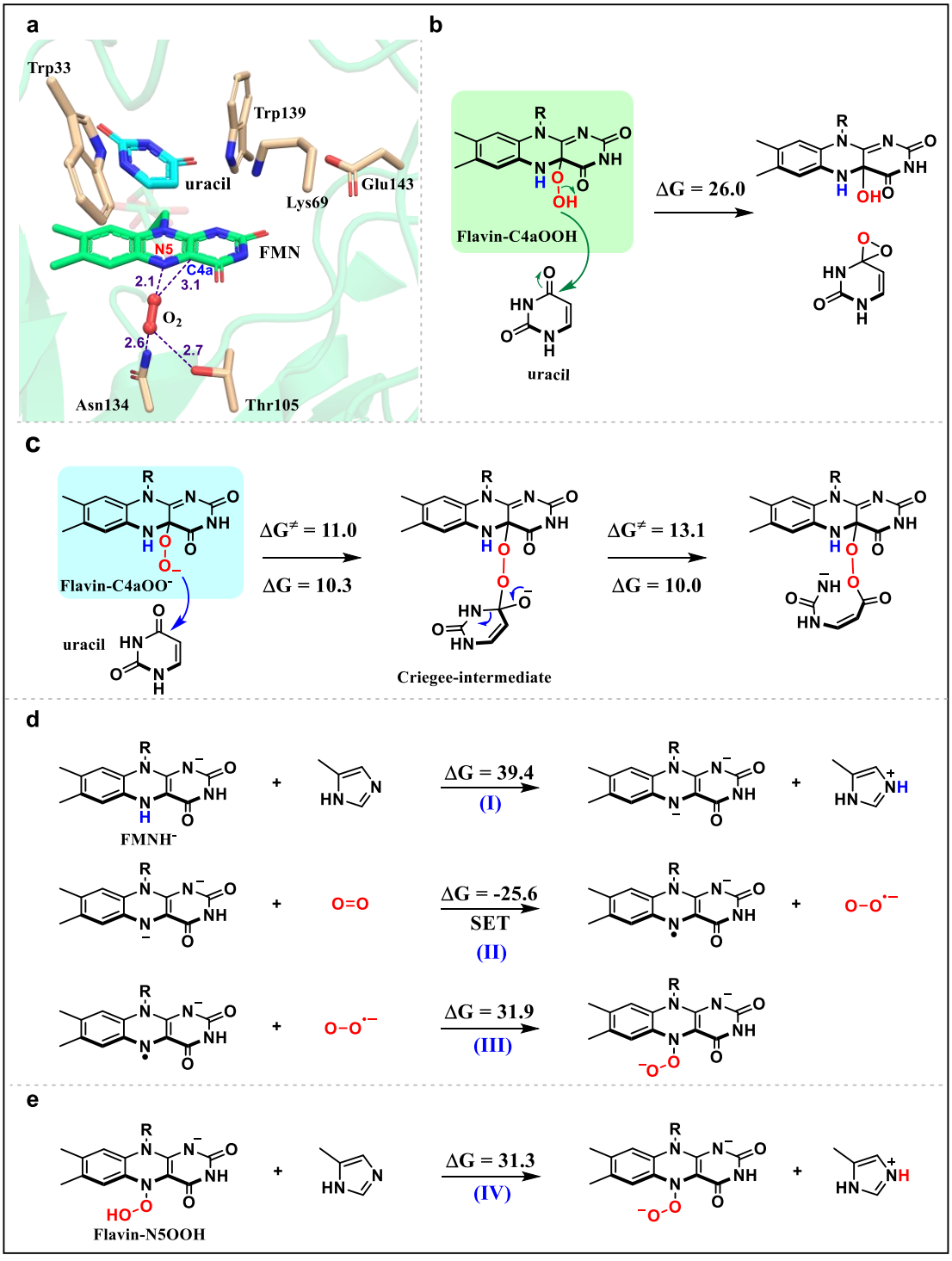

Fig. 2 | Computational evaluation of the formation of the Flavin-N5OO⁻ species. a Crystal structure of RutA in complex with uracil and O_2 (PDB ID: 6TEG). **b** QM calculated energy for Flavin-C4aOOH mediated hydroxylation of uracil. **c** QM calculated energy Flavin-C4aOO⁻ mediated C–N cleavage of uracil. **d** The formation of Flavin-N5OO⁻ initiated with the deprotonation of FMNH⁻. **e** The formation of Flavin-N5OO⁻ via deprotonation of Flavin-N5OOH species. The calculated Gibbs

reaction energy (ΔG) are given in kcal/mol.

Can the Flavin-N5OO$^-$ species be formed in flavin-enzymes?

Flavin-N5OO$^-$ was invoked as the active species for the C–N bond cleavage of uracil by RutA[53]. Various QM model calculations have been performed to test the feasibility for Flavin-N5OO$^-$ formation (Fig. 2d and Fig. 2e). As histidine residues are widely involved in proton-shuttle in flavin-enzymes, the side chain of histidine was employed during the calculations as the base. We have considered two possible routes for the formation of Flavin-N5OO$^-$ species (Fig. 2d and Fig. 2e). One is initiated with the deprotonation of the anionic flavin mononucleotide hydroquinone (FMNH$^-$), which is followed by the O_2 reduction and binding (Fig. 2d). In this route, we can see that deprotonation of FMNH$^-$ is endothermic by 39.4 kcal/mol and hence unlikely to occur. Indeed, no evidence is available to support the formation of dianion FMN species in physiological conditions. Once the dianion FMN species was formed, it can reduce O_2 readily. However, the binding of the superoxo species to the dianion FMN species is endothermic by 31.9 kcal/mol (Fig. 2d), which would make the reaction highly unfavored kinetically. In the alternative pathway, the formation of the Flavin-N5OO$^-$ species may proceed by the deprotonation of Flavin-N5OOH species (Fig. 2e). However, such process is endothermic by 31.3 kcal/mol. Thus, all these test calculations strongly indicate that the formation of Flavin-N5OO$^-$ species is highly unfavorable under physiological conditions.

The Flavin-N5OOH species functions as the powerful nucleophile for the C–N cleavage of uracil in RutA

We subsequently revisited the formation of the Flavin-N5OOH species using QM/MM calculations. An equilibrated snapshot from QM/MM MD trajectories was chosen for subsequent QM/MM calculations. Fig. 3a shows the QM/MM calculated relative energy profile for the formation of Flavin-N5OOH and the Flavin-N5OOH mediated C–N cleavage of uracil in RutA. It is seen that the reaction begins with a facile HAT from N5–H of flavin to O_2, which involves a barrier of 4.9 kcal/mol (^{3}RC → ^{3}TS1),

leading to $FMNH^{\bullet-}$/$^{\bullet}OOH$ in ^{3}INT1. To facilitate the following radical coupling reaction, the $FMNH^{\bullet-}$/$^{\bullet}OOH$ radical intermediate has to flip from its triplet to the open-shell singlet state (^{3}INT1 → ^{1}INT1$_{OS}$). Starting from ^{1}INT1$_{OS}$, we investigated two competing $^{\bullet}OOH$ rebound pathways. One is the $^{\bullet}OOH$ rebound to N5 site to form the Flavin-N5OOH species, the other is $^{\bullet}OOH$ rebound to C4a to form the flavin C4aOOH anion intermediate. QM/MM calculations show that $^{\bullet}OOH$ rebound to N5 requires a barrier of 17.9 kcal/mol (^{1}INT1$_{OS}$ →^{1}TS2$_{OS}$), affording the Flavin-N5OOH species that is 11.8 kcal/mol higher than ^{1}INT1$_{OS}$. For the rebound of $^{\bullet}OOH$ onto C4a, the reaction experiences a barrier of 15.5 kcal/mol, which gives rise to the flavin C4aOOH anion intermediate that is 10.2 kcal/mol higher than ^{1}INT1$_{OS}$ (Fig. S3). However, the reaction pathway following the flavin C4aOOH anion species are highly unfavorable kinetically (Fig. S3), indicating that the flavin C4aOOH anion specie is a dead-end along the reaction pathway.

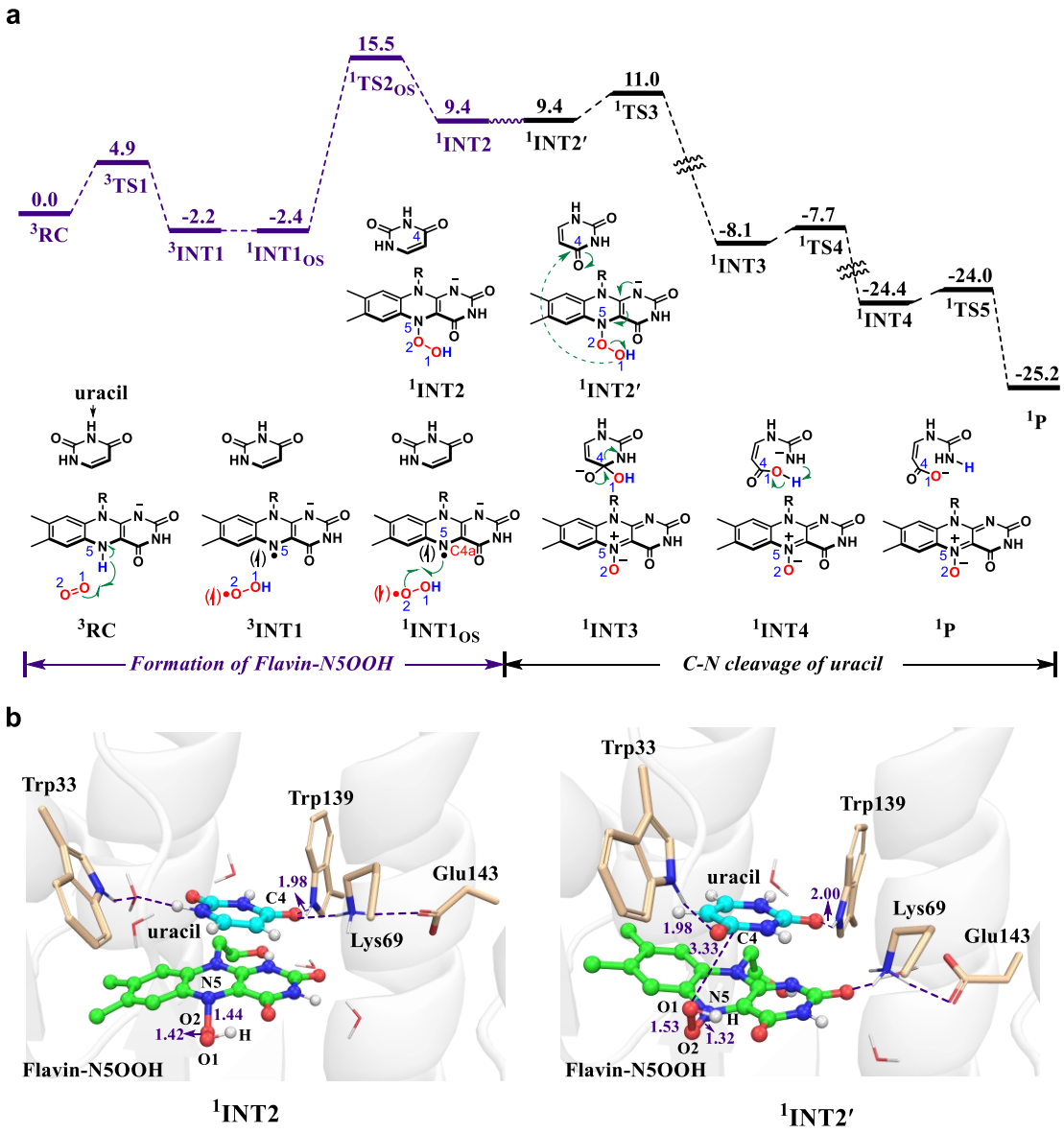

Fig. 3 | Mechanistic study of the active species formation and the C–N cleavage of uracil in RutA. a QM(UB3LYP-D3/B2)/MM calculated energy profile (in kcal/mol) for the formation of Flavin-N5OOH and the Flavin-N5OOH mediated C–N cleavage of uracil in RutA. **b** QM(UB3LYP-D3/B1)/MM optimized structures of ^{1}INT2 and ^{1}INT2′. The distances are given in Å. The superscript "3" indicates the triplet state, "1" represents the closed-shell singlet state, and the subscript "OS" represents the open-shell singlet state.

As the uracil C4 site is not well positioned toward Flavin-N5OOH species in the nascent ^{1}INT2, both the classical MD and QM/MM MD simulations have been

conducted to investigate the possible conformational change of the uracil substrate (refer to ^{1}INT2 and ^{1}INT2′ in Fig. 3b). The MD simulations show that the uracil can readily undergo the conformational change, during which the uracil rotates clockwise, leaving its C4 site in close proximity to the distal oxygen of Flavin-N5OOH species (see Movie. S1). In addition, we note that Lys69 breaks its H-bonding interactions with uracil while forming new H-bonding interactions with the negatively charged pyrimidine ring of flavin (^{1}INT2′ in Fig. 3b). The loss of the H-bond with Lys69 may render greater freedom for the rotation of uracil. After the conformational rotation, the uracil can be anchored by two H-bonds with Trp33 and Trp139, respectively. The stability of these two H-bonds has been confirmed by QM/MM MD simulations (Fig. S4).

Starting from the nascent ^{1}INT2′, the Flavin-N5OOH species can use its distal OH moiety to attack the C4 position of uracil (see the black path in Fig. 3a). The reaction is concerted (Fig. S5), with a small barrier of 1.6 kcal/mol (^{1}INT2′→ ^{1}TS3) and exothermicity of 17.5 kcal/mol (^{1}INT2′→ ^{1}IN3), and as such, the process is highly favorable both kinetically and thermodynamically. QM/MM optimized structure of ^{1}INT2 shows that O1–O2 bond has a length of 1.53Å, while the N5–O2 has a length of 1.32Å, suggesting that the O–O bond of Flavin-N5OOH is highly activated. In addition, the one-electron reduced flavin cofactor can drive efficient O–O heterolytic cleavage, leading to OH^- release and nucleophilic attack on the uracil. Once the OH^- was attached to uracil in ^{1}INT3, the following C4–N cleavage of uracil became quite facile, and proceeded with a barrier of 0.4 kcal/mol (^{1}INT3→ ^{1}TS4), thus leading to C–N cleavage in ^{1}INT4. The final intramolecular proton transfer experiences a small barrier of 0.4 kcal/mol (^{1}INT4→ ^{1}TS5), leading to the production of ^{1}P (Flavin-N5O and ureidoacrylate). Once the latter product was generated, presumably the Flavin-N5O species will undergo reduction by Nicotinamide adenine dinucleotide (NADH), leading to the intact FMN for the next catalytic cycle. The reduction of the Flavin-N5O species by NADH has been supported by our calculations (Fig. S6).

The Flavin-N5OOH functions as the powerful base in EncM

In the last section, we demonstrate that Flavin-N5OOH can act as a powerful nucleophile and cleave the C–N bond of uracil in RutA. In this section, we proceed to explore the catalytic role of Flavin-N5OOH in EncM. The X-ray crystal structure of EncM (PDB ID: 6FOQ) in complex with the flavin-adenine dinucleotide (FAD) and O_2 has been successfully crystallized (Fig. S1)[48, 50]. Starting from Flavin-N5OOH and the substrate, both the classical MD and QM/MM MD simulations were performed. QM/MM MD simulation reveals a spontaneous proton transfer within the substrate (see Sub in Fig. 4a) from O9H8 to O7 within ~200 fs, leading to the formation of Sub″ (see Fig. 4a and Fig. S7a). This is consistent with our QM model calculations, which show that the proton transfer from O9H8 to O7 is exergonic by 1.5 kcal/mol (see Fig. S7b). After the spontaneous proton transfer of Sub, a representative snapshot extracted from QM/MM MD trajectories was used for the subsequent QM/MM calculations. Fig. 4b shows the QM/MM calculated mechanism for the reactions of EncM emerging from the Flavin-N5OOH species to C4-ketone (P″). In the QM/MM optimized complex of INT2″, we can see that substrate O3H6 is in close proximity to the Flavin-N5OOH species.

Starting from INT2″, the O–O cleavage of Flavin-N5OOH species leads to the spontaneous deprotonation of O3H6 by the nascent OH^- moiety, affording a water molecule, an O3-deprotonated substrate and a Flavin-N5O species in INT3″(see Fig. 4b and Fig. 4c). Notably, the Flavin-N5O species was characterized spectroscopically in EncM[49, 50]. This step has a small barrier of 6.9 kcal/mol (INT2″→ TS3″) and an exothermicity of 35.5 kcal/mol. Next, the Flavin-N5O species can perform the electrophilic attack onto the C4 position of substrate, which involves a barrier of 13.0 kcal/mol (INT3″→INT4 ″). Starting from INT4″, the following N5−O2 cleavage is quite facile, with a small barrier of 0.9 kcal mol^{-1} (INT4″→TS5″). Then, the nascent INT5″ can evolve into the more stable species of INT5a″, during which the substrate H7 gets close to the N5 atom of flavin, while the O2 atom of flavin gets away from the N5 atom of flavin. Starting from INT5a″, the hydride transfer from the substrate C4 to the flavin N5 occurs, leading to the ketone form of the product. This process requires a barrier 15.9 kcal/mol (INT5a ″ → TS6 ″). Finally, the C4-ketone (P ″) can be converted

to the final product (PC″) via keto-enol tautomerism in water solution (see Fig. S8). Thus, the Flavin-N5OOH species functions as an efficient base in EncM, that can deprotonate the substrate O3 site thus making it electron-richer and reactive. Meanwhile, the so-formed Flavin-N5O species can act as the strong electrophile for the following oxygenation of substrate.

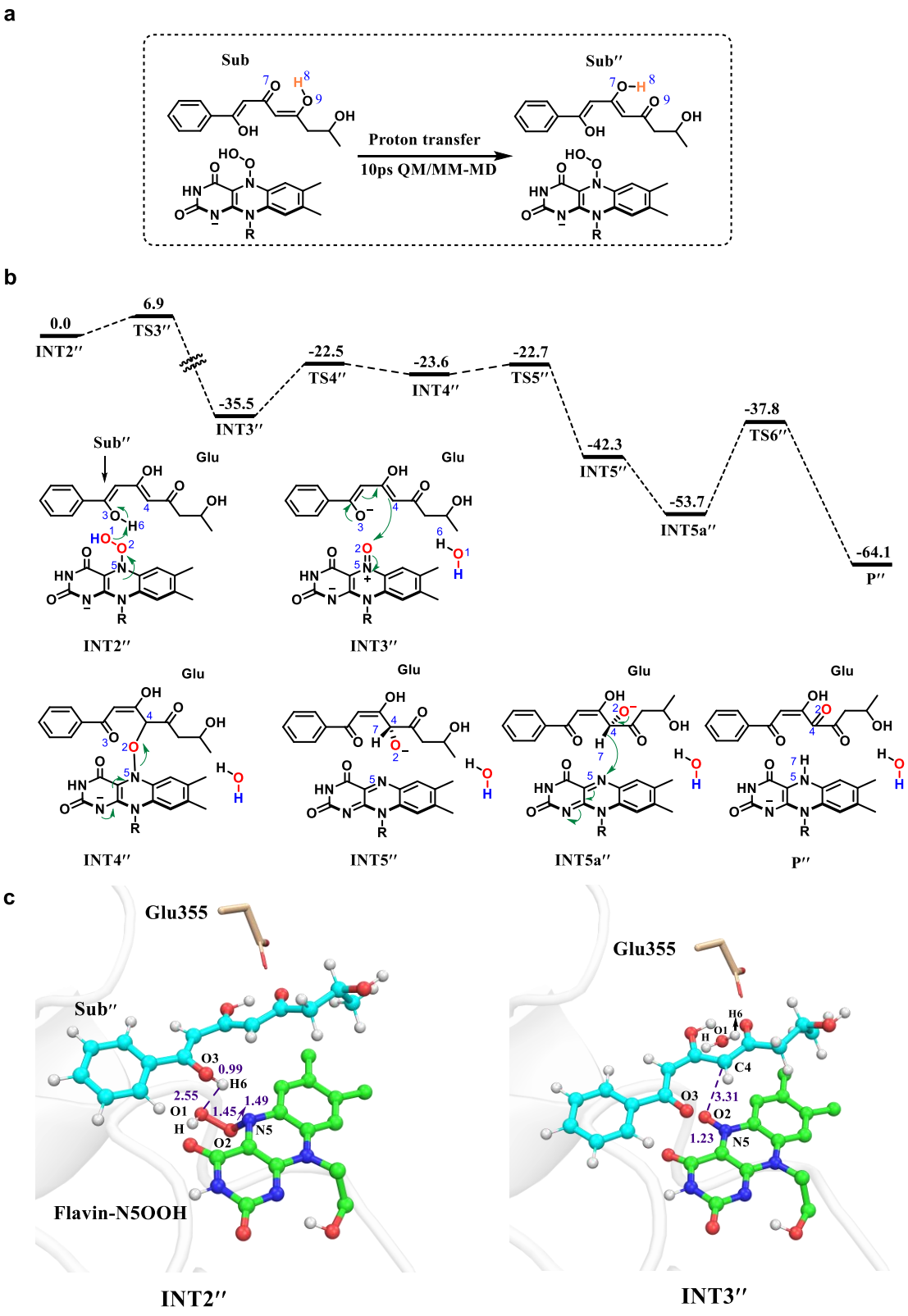

Fig. 4 | Mechanistic study of the active species formation and the substrate deprotonation in EncM. a The spontaneous proton transfer of Sub to form Sub″ during the QM/MM MD simulations. **b** QM(UB3LYP-D3/B2)/MM calculated energy profile (in kcal/mol) for the Flavin-N5OOH mediated substrate deprotonation in EncM.

c QM(UB3LYP-D3/B2)/MM optimized structures of INT2″ and INT3″. The distances are given in Å.

Flavin-N5OOH: the prevalent nucleophile in superfamily of flavoenzymes

The hydroxide (OH^-) ion is considered to be one of the strongest nucleophiles in chemistry. For comparison, we have investigated the OH^--catalyzed hydrolysis of uracil in water solution with cluster-continuum model calculations[59] (see Fig. 5a and Fig. S9) . Our calculations show that OH^- mediated hydrolysis of uracil involves a high barrier of 26.0 kcal/mol and an endothermicity of 22.0 kcal/mol (see Fig. 5a). As such, the process is unfavorable both kinetically and thermodynamically. In terms of Flavin-N5OOH mediated C–N cleavage of uracil, the process involves a small barrier of 1.6 kcal/mol (^{1}INT2′→ ^{1}TS3 refer to Fig. 3a) and exothermicity of 17.5 kcal/mol (^{1}INT2′→ ^{1}IN3 refer to Fig. 3a). Thus, the Flavin-N5OOH species functions as a much stronger nucleophile and base compared with the OH^- species. This is primarily because the solvated OH^- is significantly stabilized by extensive H-bonding interactions with surrounding waters[60] (see Fig. S9). Unlike the solvated OH^- ion, the OH-moiety in the Flavin-N5OOH species is weakly bonded to the Flavin-N5O species, which makes the Flavin-N5OOH species highly reactive in nucleophilic additions.

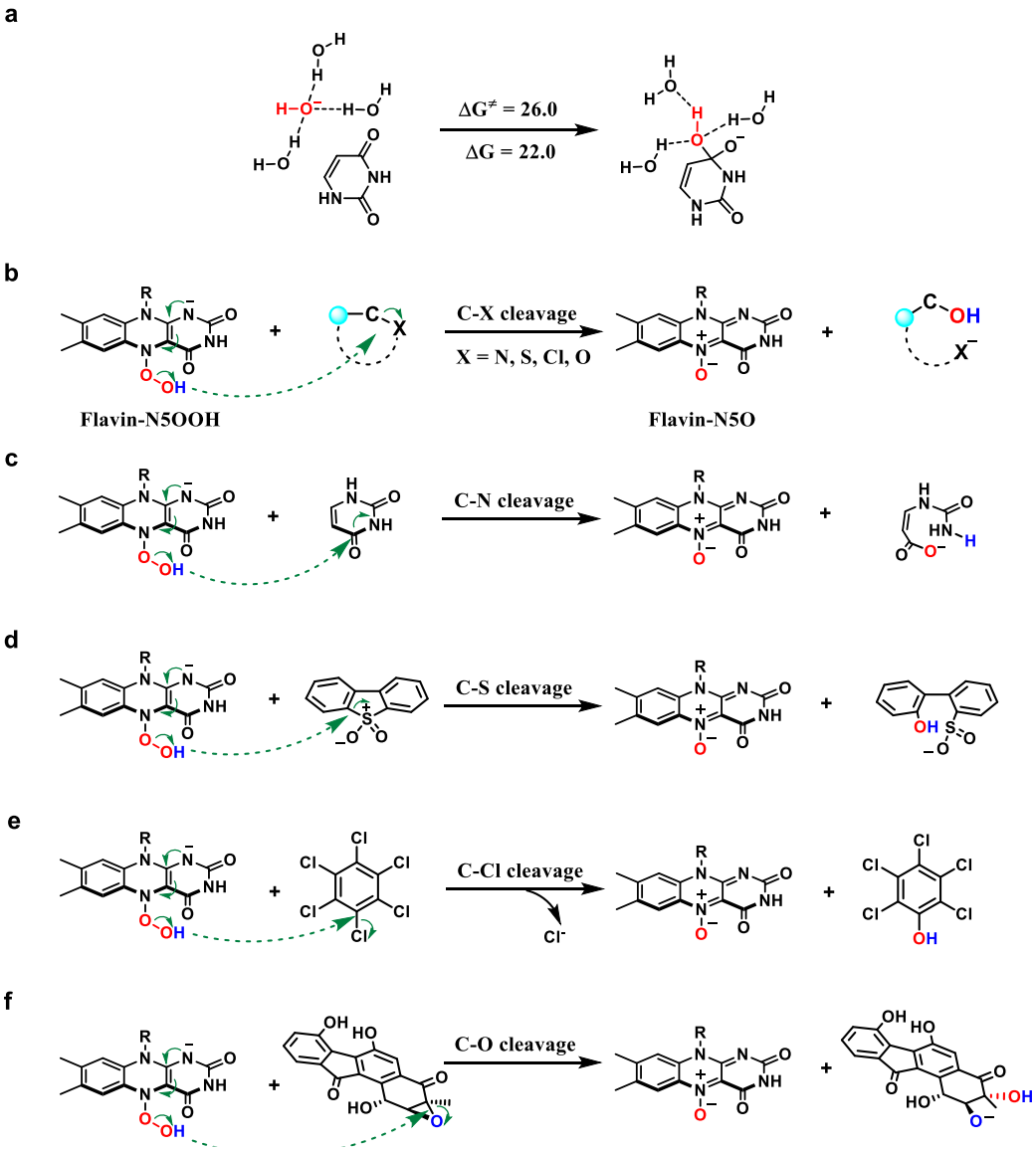

Fig. 5 | Calculated energy barrier and reaction energy (in kcal/mol) for OH^- nucleophilic attack on uracil substrate in bulk solvent and proposed catalytic mechanisms of Flavin-N5OOH-mediated C–X (X=N, S, Cl, O) cleavage of substrates: a Calculated energy barrier and reaction energy (in kcal/mol) for OH^- nucleophilic attack on uracil in bulk solvent. **b** A general mechanism of Flavin-N5OOH-mediated C–X bond cleavage. **c** Flavin-N5OOH-mediated C–N bond cleavage of uracil catalyzed by RutA. **d** Proposed mechanism of the C–S bond cleavage of dibenzothiophene sulfone catalyzed by DszA. **e** Proposed mechanism of the C–Cl bond cleavage (dehalogenation) of hexachlorobenzene catalyzed by HcbA1. **f** Proposed mechanism for the epoxide ring-opening of fluostatin C in the presence of FAD and

NADH.

In addition to its high reactivity, the protein environment enables the specific selectivity for the Flavin-N5OOH mediated nucleophilic addition or base reactions, as demonstrated in the catalysis of RutA and EncM. Such selectivity is otherwise challenging to realize with the solvated "OH^-". We expect that Flavin-N5OOH can function as the common active species in the cleavage of the C–X (X=N, S, Cl, O) bond of the various substrates in flavoenzyme (Fig. 5b). In addition to the C–N cleavage of uracil catalyzed by RutA in this work (Fig. 5c), other examples may include the C–S bond cleavage of dibenzothiophene sulfone catalyzed by the flavoenzyme DszA (Fig. 5d)[61], flavin-dependent dehalogenation[62, 63] (Fig. 5e) and even in nonenzymatic epoxide ring-opening of fluostatin C mediated by FAD and NADH (Fig. 5f)[64]. All these types of reactions have been supported by our QM model calculations (Figure S10~S12).

Conclusion

In summary, extensive computational studies were performed to elucidate the active species for RutA-catalyzed C–N cleavage of uracil and EncM-catalyzed C4-ketolation. Our study shows that the flavin-N5OOH species is in fact the common active species in both flavoenzyme RutA and EncM. In RutA, the flavin-N5OOH species functions as a powerful nucleophile for the selective C–N cleavage of uracil, while in EncM it acts as an efficient base in selective deprotonation of substrate, which produces the electrophile Flavin-N5O and simultaneously makes the substrate more nucleophilic. These unique reactivities of flavin-N5OOH are too challenging to realize with the solvated base of "OH^-". We expect that flavin-N5OOH can either function as a base for the selective deprotonation or as a powerful nucleophile in mediating the cleavage of C–X (X=N, S, Cl, O) bonds in biology. As such, this study broadens significantly our understanding of the O_2 activation chemistry by flavin enzymes.

Methods

System Setup

The initial structure of RutA complexed with uracil and O_2 were prepared based on the crystal structure (PDB ID: 6TEG)[53]. Missing residues (residue ID: 292-310) were added through SWISS-MODEL (available at: swissmodel.expasy.org). The protonation state of titratable residues was assigned on the basis of pK_a values from the PROPKA program[65] in combination with the careful visual inspection of local hydrogen-bonded networks. Histidine residues 38, 58, and 60 were protonated at the δ position, while histidine residues 82, 277 and 373 were protonated at the ε position. All glutamic acid and aspartic acid residues were deprotonated. For the setup the EncM system, the initial structure of EncM complexed with and O_2 were prepared based on the crystal structure (PDB ID: 6FOQ)[50]. The substrate was docked into the active site using AutoDock Vina[66]. Only chain A was kept while chains B, C and D were omitted. Histidines (His or H) 236, 291, 296, 343, and 411 were protonated at the δ position, while histidines 78, 83, 127, 138, 209, 264, 280 and 397 were protonated at the ε position. All glutamic acid (Glu or E) and aspartic acid (Asp or D) residues were deprotonated. The AMBER ff14SB force field was employed for the protein residues[67]. The general AMBER force field (gaff)[68]was used to generate the parameters for the different forms of the $FMNH^-$, Flavin-N5OOH, uracil, Sub and O_2 with the partial atomic charges obtained from the RESP method[69] at the B3LYP/6-31G(d) level of theory. The parmchk2 utility from AmberTools18 was used to generate the missing parameters. Counter ions (Na^+) were added to neutralize the total charge of the system. The resulting system was solvated in a rectangular box of TIP3P water extending up to a minimum distance of 16 Å from the protein surface.

MD Simulation

After the setup, the systems were fully minimized by a combination of steepest descent and subsequent conjugate gradient methods. The systems were annealed from 0 to 300 K for 50 ps using with the NVT ensemble, during which the constraint of 15 kcal/mol/Å was applied. Then, the density equilibration for 1.0 ns was conducted under the NPT ensemble to obtain a uniform density, where the target temperature of 300 K was kept with the Langevin thermostat and a 2 ps collision frequency, and the 1.0 atm target

pressure was maintained with the Berendsen barostat and a pressure relaxation time of 1 ps. In RutA and EncM, the positions of O_2 are restrained with a restraint of 25 kcal/mol/A during equilibration and 200 ns production MD simulations, thus avoiding their diffusion into the bulk water. During the simulations, the covalent bonds involving hydrogen atoms were constrained with the SHAKE method, and the integration step was set to 2 fs. All MD simulations were performed using Amber 18 software package[70].

QM/MM Calculations

Representative snapshots according to the clustering analysis of MD trajectory (Fig. S4 and Fig. S13~S17) were used for subsequent QM/MM MD simulations. Firstly, the selected snapshot was subject to the QM/MM MD simulation for 10ps to get more accurate structures. Then, the representative snapshot from the QM/MM MD trajectory was selected for the QM/MM calculations with ChemShell software[71, 72], which combines Turbomole[73] for the QM region and DL_POLY[74] for the MM region. The polarizing effect of the protein environment on the QM region was treated with the electrostatic embedding scheme. Hydrogen link atoms with the charge-shift model were exploited to deal with the QM/MM boundary. During the QM/MM calculations, the hybrid UB3LYP[75] functional was used for the QM region, while the same Amber force field was used for the MM region. The double-ζ basis set def2-SVP(B1) was used for geometry optimizations, while the def2-TZVP(B2) basis set was employed for the single-point energy calculations. The dispersion corrections computed with Grimme's D3 method[76, 77] were considered in all QM/MM calculations.

Data availability

Data relating to computational calculations are available in the Supplementary Information or from the authors upon reasonable request. All QM/MM and QM calculated energy profiles, structures, as well as cartesian coordinates of the QM region for all computed species are available in the Supplementary Data.

REFERENCES

1. Macheroux P., Kappes B.&Ealick S. E. Flavogenomics--a genomic and structural view of flavin-dependent proteins. *FEBS J.* **278**, 2625-2634 (2011).
2. Walsh C. T.&Wencewicz T. A. Flavoenzymes: versatile catalysts in biosynthetic pathways. *Nat. Prod. Rep.* **30**, 175-200 (2013).
3. Heine T., van Berkel W. J. H., Gassner G., van Pee K. H.&Tischler D. Two-Component FAD-Dependent Monooxygenases: Current Knowledge and Biotechnological Opportunities. *Biology* **7**, 42 (2018).
4. Teufel R. Flavin-catalyzed redox tailoring reactions in natural product biosynthesis. *Arch. Biochem. Biophys.* **632**, 20-27 (2017).
5. Teufel R., Agarwal V.&Moore B. S. Unusual flavoenzyme catalysis in marine bacteria. *Curr. Opin. Chem. Biol.* **31**, 31-39 (2016).
6. Massey V. Activation of molecular oxygen by flavins and flavoproteins. *J. Biol. Chem.* **269**, 22459-22462 (1994).
7. Romero E., Gómez Castellanos J. R., Gadda G., Fraaije M. W.&Mattevi A. Same Substrate, Many Reactions: Oxygen Activation in Flavoenzymes. *Chem. Rev.* **118**, 1742-1769 (2018).
8. Ghisla S.&Massey V. Mechanisms of flavoprotein-catalyzed reactions. *Eur. J. Biochem.* **181**, 1-17 (1989).
9. Bruice T. C. Mechanisms of flavin catalysis. *Acc. Chem. Res.* **13**, 256-262 (1980).
10. Mansoorabadi S. O., Thibodeaux C. J.&Liu H.-w. The Diverse Roles of Flavin CoenzymesNature's Most Versatile Thespians. *J. Org. Chem.* **72**, 6329-6342 (2007).
11. Huijbers M. M., Montersino S., Westphal A. H., Tischler D.&van Berkel W. J. Flavin dependent monooxygenases. *Arch. Biochem. Biophys.* **544**, 2-17 (2014).
12. Chaiyen P., Fraaije M. W.&Mattevi A. The enigmatic reaction of flavins with oxygen. *Trends Biochem. Sci.* **37**, 373-380 (2012).
13. Fitzpatrick P. F. Substrate Dehydrogenation by Flavoproteins. *Acc. Chem. Res.* **34**, 299-307 (2001).
14. Ghisla S.&Thorpe C. Acyl-CoA dehydrogenases. A mechanistic overview. *Eur. J. Biochem.* **271**, 494-508 (2004).
15. Ouedraogo D. et al. Amine oxidation by d-arginine dehydrogenase in Pseudomonas aeruginosa. *Arch. Biochem. Biophys.* **632**, 192-201 (2017).
16. Paul C. E., Eggerichs D., Westphal A. H., Tischler D.&van Berkel W. J. H. Flavoprotein monooxygenases: Versatile biocatalysts. *Biotechnol. Adv.* **51**, 107712 (2021).
17. van Berkel W. J., Kamerbeek N. M.&Fraaije M. W. Flavoprotein monooxygenases, a diverse class of oxidative biocatalysts. *J. Biotechnol.* **124**, 670-689 (2006).
18. Leisch H., Morley K.&Lau P. C. Baeyer-Villiger monooxygenases: more than just green chemistry. *Chem. Rev.* **111**, 4165-4222 (2011).
19. de Gonzalo G., Mihovilovic M. D.&Fraaije M. W. Recent developments in the application of Baeyer-Villiger monooxygenases as biocatalysts. *Chembiochem* **11**, 2208-2231 (2010).
20. Ellis H. R. The FMN-dependent two-component monooxygenase systems. *Arch. Biochem. Biophys.* **497**, 1-12 (2010).
21. Chenprakhon P., Wongnate T.&Chaiyen P. Monooxygenation of aromatic compounds by flavin-dependent monooxygenases. *Protein Sci.* **28**, 8-29 (2019).

22. Andorfer M. C.&Lewis J. C. Understanding and Improving the Activity of Flavin-Dependent Halogenases via Random and Targeted Mutagenesis. *Annu. Rev. Biochem.* **87**, 159-185 (2018).
23. Phintha A., Prakinee K.&Chaiyen P. Structures, mechanisms and applications of flavin-dependent halogenases. *Enzymes* **47**, 327-364 (2020).
24. Agarwal V. et al. Enzymatic Halogenation and Dehalogenation Reactions: Pervasive and Mechanistically Diverse. *Chem. Rev.* **117**, 5619-5674 (2017).
25. Blasiak L. C.&Drennan C. L. Structural Perspective on Enzymatic Halogenation. *Acc. Chem. Res.* **42**, 147-155 (2009).
26. Prakinee K. et al. Mechanism-guided tunnel engineering to increase the efficiency of a flavin-dependent halogenase. *Nat. Catal.* **5**, 534-544 (2022).
27. Sorigué D. et al. An algal photoenzyme converts fatty acids to hydrocarbons. *Science* **357**, 903-907 (2017).
28. Heelis P. F. The photophysical and photochemical properties of flavins (isoalloxazines). *Chem. Soc. Rev.* **11**, 15-39 (1982).
29. Harrison W., Huang X.&Zhao H. Photobiocatalysis for Abiological Transformations. *Acc. Chem. Res.* **55**, 1087-1096 (2022).
30. Sandoval B. A., Kurtoic S. I., Chung M. M., Biegasiewicz K. F.&Hyster T. K. Photoenzymatic Catalysis Enables Radical-Mediated Ketone Reduction in Ene-Reductases. *Angew. Chem. Int. Ed. Engl.* **58**, 8714-8718 (2019).
31. Huang X. et al. Photoenzymatic enantioselective intermolecular radical hydroalkylation. *Nature* **584**, 69-74 (2020).
32. Solomon E. I. et al. Copper active sites in biology. *Chem. Rev.* **114**, 3659-3853 (2014).
33. Huang X.&Groves J. T. Oxygen Activation and Radical Transformations in Heme Proteins and Metalloporphyrins. *Chem. Rev.* **118**, 2491-2553 (2018).
34. Shaik S. et al. P450 enzymes: their structure, reactivity, and selectivity-modeled by QM/MM calculations. *Chem. Rev.* **110**, 949-1017 (2010).
35. Walsh C. Flavin coenzymes: at the crossroads of biological redox chemistry. *Acc. Chem. Res.* **13**, 148-155 (1980).
36. Luo Y.&Liu Y.-J. Revisiting the Origin of Bacterial Bioluminescence: QM/MM Study on Oxygenation Reaction of Reduced Flavin in Protein. *ChemPhysChem* **20**, 405-409 (2019).
37. Badieyan S., Bach R. D.&Sobrado P. Mechanism of N-hydroxylation catalyzed by flavin-dependent monooxygenases. *J. Org. Chem.* **80**, 2139-2147 (2015).
38. Palfey B. A.&McDonald C. A. Control of catalysis in flavin-dependent monooxygenases. *Arch. Biochem. Biophys.* **493**, 26-36 (2010).
39. Mattevi A. To be or not to be an oxidase: challenging the oxygen reactivity of flavoenzymes. *Trends Biochem. Sci.* **31**, 276-283 (2006).
40. Fraaije M. W.&Mattevi A. Flavoenzymes: diverse catalysts with recurrent features. *Trends Biochem. Sci.* **25**, 126-132 (2000).
41. Polyak I., Reetz M. T.&Thiel W. Quantum mechanical/molecular mechanical study on the mechanism of the enzymatic Baeyer-Villiger reaction. *J. Am. Chem. Soc.* **134**, 2732-2741 (2012).
42. Tweedy S. E. et al. Hydroxyl Radical-Coupled Electron-Transfer Mechanism of Flavin-Dependent Hydroxylases. *J. Phys. Chem. B* **123**, 8065-8073 (2019).
43. Barbosa A. C. C., Neves R. P. P., Sousa S. F., Ramos M. J.&Fernandes P. A. Mechanistic Studies of a Flavin Monooxygenase: Sulfur Oxidation of Dibenzothiophenes by DszC. *ACS Catal.* **8**, 9298-

9311 (2018).
44. Fürst M. J. L. J., Gran-Scheuch A., Aalbers F. S.&Fraaije M. W. Baeyer–Villiger Monooxygenases: Tunable Oxidative Biocatalysts. *ACS Catal.* **9**, 11207-11241 (2019).
45. Ridder L., Mulholland A. J., Rietjens I. M. C. M.&Vervoort J. A Quantum Mechanical/Molecular Mechanical Study of the Hydroxylation of Phenol and Halogenated Derivatives by Phenol Hydroxylase. *J. Am. Chem. Soc.* **122**, 8728-8738 (2000).
46. Ridder L., Harvey J. N., Rietjens I. M. C. M., Vervoort J.&Mulholland A. J. Ab Initio QM/MM Modeling of the Hydroxylation Step in p-Hydroxybenzoate Hydroxylase. *J. Phys. Chem. B* **107**, 2118-2126 (2003).
47. Teufel R. Preparation and Characterization of the Favorskiiase Flavoprotein EncM and Its Distinctive Flavin-N5-Oxide Cofactor. *Meth. Enzymol.* **604**, 523-540 (2018).
48. Saleem-Batcha R. et al. Enzymatic control of dioxygen binding and functionalization of the flavin cofactor. *Proc. Natl. Acad. Sci. U. S. A.* **115**, 4909-4914 (2018).
49. Teufel R. et al. Biochemical Establishment and Characterization of EncM's Flavin-N5-oxide Cofactor. *J. Am. Chem. Soc.* **137**, 8078-8085 (2015).
50. Teufel R. et al. Flavin-mediated dual oxidation controls an enzymatic Favorskii-type rearrangement. *Nature* **503**, 552-556 (2013).
51. Cheng Q., Xiang L., Izumikawa M., Meluzzi D.&Moore B. S. Enzymatic total synthesis of enterocin polyketides. *Nat. Chem. Biol.* **3**, 557-558 (2007).
52. Xiang L., Kalaitzis J. A.&Moore B. S. EncM, a versatile enterocin biosynthetic enzyme involved in Favorskii oxidative rearrangement, aldol condensation, and heterocycle-forming reactions. *Proc. Natl. Acad. Sci. U.S.A.* **101**, 15609-15614 (2004).
53. Matthews A. et al. Aminoperoxide adducts expand the catalytic repertoire of flavin monooxygenases. *Nat. Chem. Biol.* **16**, 556-563 (2020).
54. Adak S.&Begley T. P. RutA-Catalyzed Oxidative Cleavage of the Uracil Amide Involves Formation of a Flavin-N5-oxide. *Biochemistry* **56**, 3708-3709 (2017).
55. Duan Y. et al. A Flavoprotein Dioxygenase Steers Bacterial Tropone Biosynthesis via Coenzyme A-Ester Oxygenolysis and Ring Epoxidation. *J. Am. Chem. Soc.* **143**, 10413-10421 (2021).
56. Toplak M., Matthews A.&Teufel R. The devil is in the details: The chemical basis and mechanistic versatility of flavoprotein monooxygenases. *Arch. Biochem. Biophys.* **698**, 108732 (2021).
57. Matthews A. et al. Bacterial flavoprotein monooxygenase YxeK salvages toxic S-(2-succino)-adducts via oxygenolytic C-S bond cleavage. *FEBS J.* **289**, 787-807 (2022).
58. Toplak M.&Teufel R. Three Rings to Rule Them All: How Versatile Flavoenzymes Orchestrate the Structural Diversification of Natural Products. *Biochemistry* **61**, 47-56 (2022).
59. Wang B., Cao Z., Sharon D. A.&Shaik S. Computations Reveal a Rich Mechanistic Variation of Demethylation of N-Methylated DNA/RNA Nucleotides by FTO. *ACS Catal.* **5**, 7077-7090 (2015).
60. Tuckerman M., Laasonen K., Sprik M.&Parrinello M. Ab Initio Molecular Dynamics Simulation of the Solvation and Transport of H3O+ and OH- Ions in Water. *J. Phys. Chem. C* **99**, 5749-5752 (1995).
61. Adak S.&Begley T. P. Dibenzothiophene Catabolism Proceeds via a Flavin-N5-oxide Intermediate. *J. Am. Chem. Soc.* **138**, 6424-6426 (2016).
62. Adak S.&Begley T. P. Hexachlorobenzene Catabolism Involves a Nucleophilic Aromatic Substitution and Flavin-N5-Oxide Formation. *Biochemistry* **58**, 1181-1183 (2019).
63. Takagi K. et al. Aerobic mineralization of hexachlorobenzene by newly isolated

pentachloronitrobenzene-degrading Nocardioides sp. strain PD653. *Appl. Environ. Microbiol.* **75**, 4452-4458 (2009).
64. Yang C. et al. Biochemical and structural insights of multifunctional flavin-dependent monooxygenase FlsO1-catalyzed unexpected xanthone formation. *Nat. Commun.* **13**, 5386 (2022).
65. Sondergaard C. R., Olsson M. H., Rostkowski M.&Jensen J. H. Improved Treatment of Ligands and Coupling Effects in Empirical Calculation and Rationalization of pKa Values. *J. Chem. Theory Comput.* **7**, 2284-2295 (2011).
66. Trott O.&Olson A. J. AutoDock Vina: Improving the speed and accuracy of docking with a new scoring function, efficient optimization, and multithreading. *J. Comput. Chem.* **31**, 455-461 (2010).
67. Maier J. A. et al. ff14SB: Improving the Accuracy of Protein Side Chain and Backbone Parameters from ff99SB. *J. Chem. Theory Comput.* **11**, 3696-3713 (2015).
68. Wang J., Wolf R. M., Caldwell J. W., Kollman P. A.&Case D. A. Development and testing of a general amber force field. *J. Comput. Chem.* **25**, 1157-1174 (2004).
69. Bayly C. I., Cieplak P., Cornell W.&Kollman P. A. A well-behaved electrostatic potential based method using charge restraints for deriving atomic charges: the RESP model. *J. Phys. Chem. C* **97**, 10269-10280 (1993).
70. Case, D. A. et al. Amber (2018); https://ambermd.org/.
71. Metz S., Kästner J., Sokol A. A., Keal T. W.&Sherwood P. ChemShell—a modular software package for QM/MM simulations. *WIREs Comput. Mol. Sci.* **4**, 101-110 (2014).
72. Lu Y. et al. Multiscale QM/MM modelling of catalytic systems with ChemShell. *Phys. Chem. Chem. Phys.*, (2023).
73. Furche F. et al. Turbomole. *WIREs Comput. Mol. Sci.* **4**, 91-100 (2014).
74. Smith W., Yong C. W.&Rodger P. M. DL_POLY: Application to molecular simulation. *Mol. Simul.* **28**, 385-471 (2002).
75. Becke A. D. Density‐functional thermochemistry. III. The role of exact exchange. *J. Chem. Phys.* **98**, 5648-5652 (1993).
76. Grimme S. Semiempirical GGA-type density functional constructed with a long-range dispersion correction. *J. Comput. Chem.* **27**, 1787-1799 (2006).
77. Grimme S., Ehrlich S.&Goerigk L. Effect of the damping function in dispersion corrected density functional theory. *J. Comput. Chem.* **32**, 1456-1465 (2011).

Acknowledgements B.W is supported by the National Natural Science Foundation of China (22122305, 22121001 and 21933009). S.S. is supported by the Israel Science Foundation (ISF, grant 520/18).

Author contributions B.W conceived and supervised the project. Q.Z performed most of computational work, with partial contribution from Q.C. Q.Z, B.W. and S.S. cowrote the manuscript.

Competing interests Authors declare no competing interests.

Additional information

Supplementary information is available for this paper at https:

Correspondence and requests for materials should be addressed to S.S or B.W.